SUPPLEMENTARY MATERIAL:

Room Temperature Optically Pumped GeSn Microdisk Lasers

J. Chrétien[1,a)], Q. M. Thai[1], M. Frauenrath[2], L. Casiez[2], A. Chelnokov[2], V. Reboud[2], J.M. Hartmann[2], M. El Kurdi[3], N. Pauc[1], V. Calvo[1]

[1]*Univ. Grenoble Alpes, CEA, Grenoble INP, IRIG, PHELIQS, Grenoble, France*

[2]*Univ. Grenoble Alpes, CEA, LETI, Grenoble, France*

[3] *Université Paris-Saclay, CNRS, C2N, 10 boulevard Thomas Gobert, 91120 Palaiseau, France*

a) Corresponding author: jeremie.chretien@outlook.com

A. Reciprocal space mapping (RSM)

X-ray diffraction mapping around (004) (not shown here) and (224) asymmetric order gave us the tin content and the macroscopic degree of strain relaxation. They are provided in **Table S1**. The extraction protocol was the same than in Refs.[1,2,3]

TABLE S1. Sn content and macroscopic degree of strain relaxation found in RSM.

x_{Sn} (%)	*R (%)*
7.4% (lower part)	91
Transition layer	
14.1%	96
17.2%	73
16.1%	76

B. Thermal simulations

Thermal simulations under continuous waves (CW) were performed using a 2D axisymmetric model from COMSOL software. For both simulations, the temperature of the bottom substrate was fixed to 293 K as a boundary condition, justified experimentally by the good thermal exchange with the temperature controller. The surface heating flow was applied on the top surface. We assumed that all the input power density was converted into heat. Since the sample was placed under vacuum, the other thermal exchanges were indeed supposed to be negligible. Material parameters such as the thermal conductivity k, the thermal capacity C_P and the density ρ used for simulations are given in **Table S2**. The GeSn thermal conductivity was supposed to be $1.65\ W.m^{-1}\ K^{-1}$. This value was obtained through an extrapolation from the experimental thermal conductivity study from Spirito et al[4].

TABLE S2. Material parameters for FEM simulation

Material	k ($W.m^{-1}\ K^{-1}$)	C_p ($J.kg^{-1}K^{-1}$)	ρ ($kg.m^{-3}$)

$GeSn$	1.65	310	5323
Ge	58	310	5323
AlN^{24}	285	741	3255
$Si\ (Wafer)$	131	700	2329

Geometrical parameters were derived from SEM images. They are defined and gathered in **Table S3**. Various disk under-etches ($u_{underetch}$), pedestal heights (t_{height}) and materials were investigated during CW simulations to quantify the impact of each parameter.

TABLE S3. Geometrical parameters for FEM simulation

r_{disk}
t_{GeSn}
Disk
$u_{underetch}$
$t_{pedestal}$
Pedestal
Wafer

	GeSn on Ge pedestal	GeSn on AlN pedestal
t_{GeSn}	900 nm	800 nm
$t_{pedestal}$	2.5 µm	0.540 µm
r_{disk}	7.5 µm	7.5 µm
$u_{underetch}$	3.5 µm	1.55 µm

Pumping power density was set at 1 kW.cm^{-2}. Results are presented in **fig S1 (a).** The so called “edge temperature” was taken close to the edge of the disk, at 0.5 µm from the edge, near the mode region. The better thermal dissipation was obtained with the lowest undercut (1.5 µm), the lowest pedestal height (0.5 µm) and the highest material conductivity of the pedestal (AlN, here). In that case, the edge temperature was 307.8 K. An increase of the underetch, from 1.5 µm to 3.5 µm, while keeping the other parameters the same, drastically increased the edge temperature to 365 K. The distance between the thermal sink (i.e. the disk pedestal) and the edges indeed had a major impact on thermal dissipation because of the low heat conductivity of GeSn compared to Ge. Reducing the pedestal height from 2.5 µm down to 0.5 µm or replacing AlN by Ge otherwise had a minor impact on the edge temperature rise.

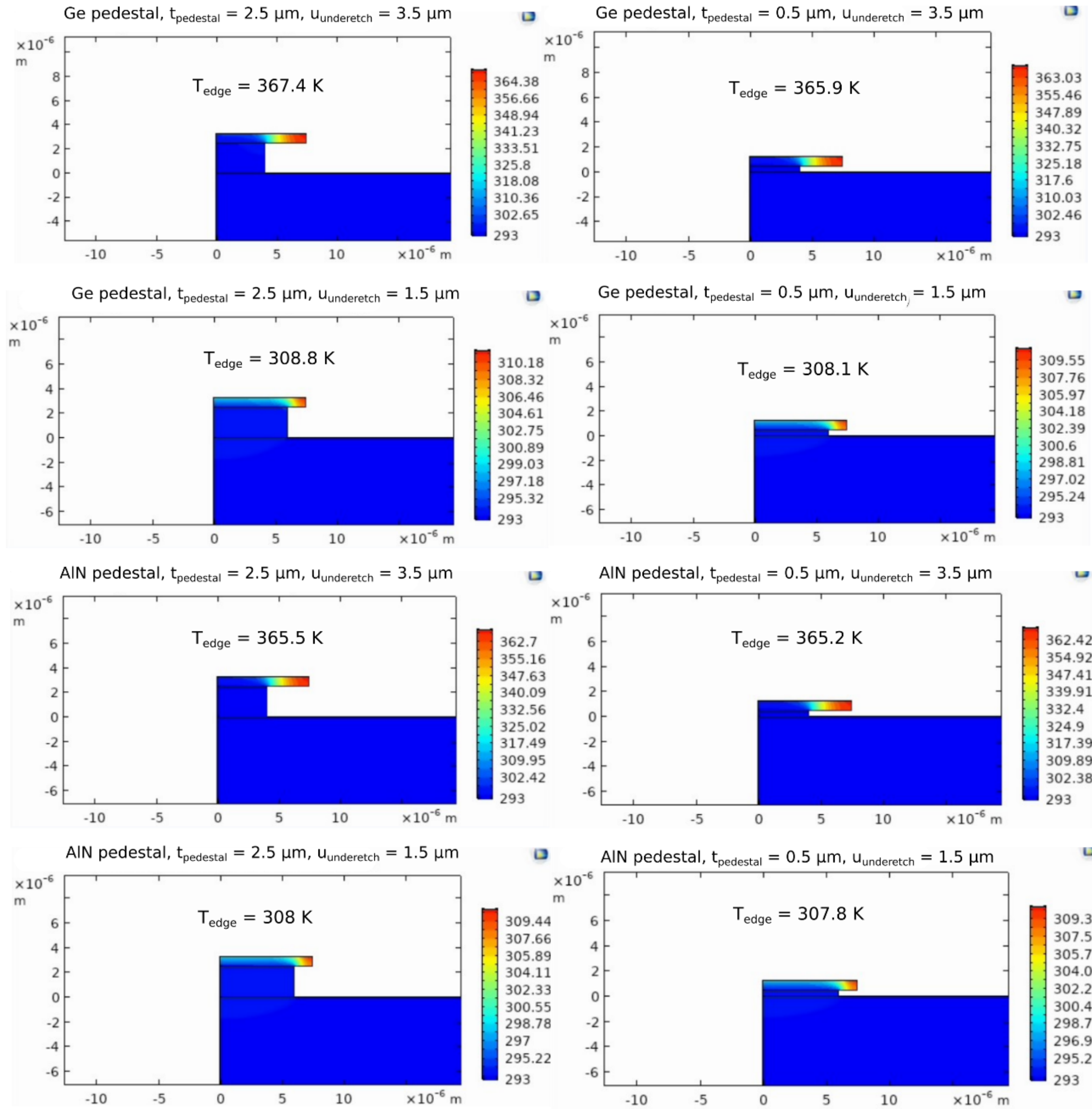

FIG. S1. Thermal profile under continous waves pumping (1 kW/cm²) for 15 µm diameter GeSn disks on Ge (left) and AlN (right) pedestals.

To conclude, thermal management using a suitable configuration (undercut, pedestal height or material conductivity) helps in reaching higher lasing temperatures under these high pumping power conditions, in good agreement with recent work[5].

C. Additional optical spectrum and Light in – Light out curve.

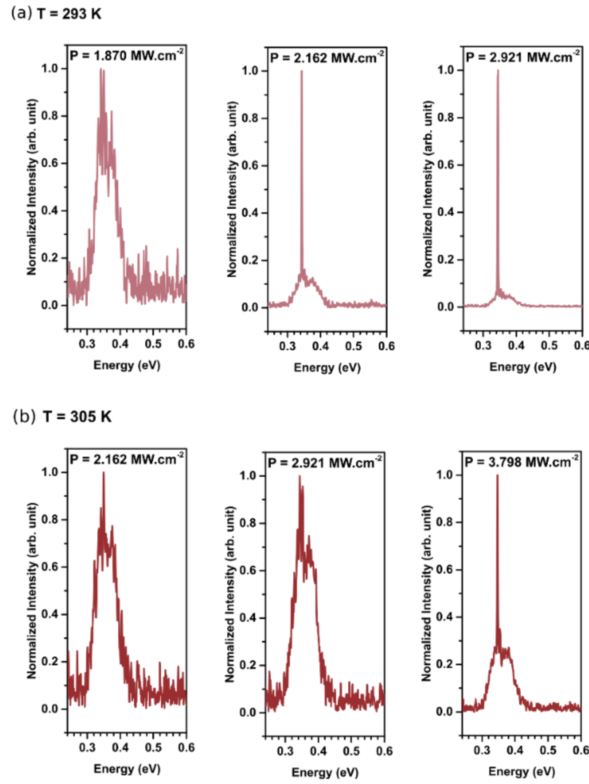

FIG. S2. Additionnal spectrum at 293K and 305K for 15 µm diameter GeSn disk on AlN below, near and above the threshold.

Extra optical spectrum is provided in **fig. S2** for the GeSn disk on AlN pedestal for 293 K and 305 K. Lasing peak appears from photoluminescence when the input power density increases. The thresholds for 293 K and 305 K are estimated at 2.1 MW.cm^{-2} and 3.3 MW. cm^{-2} respectively.

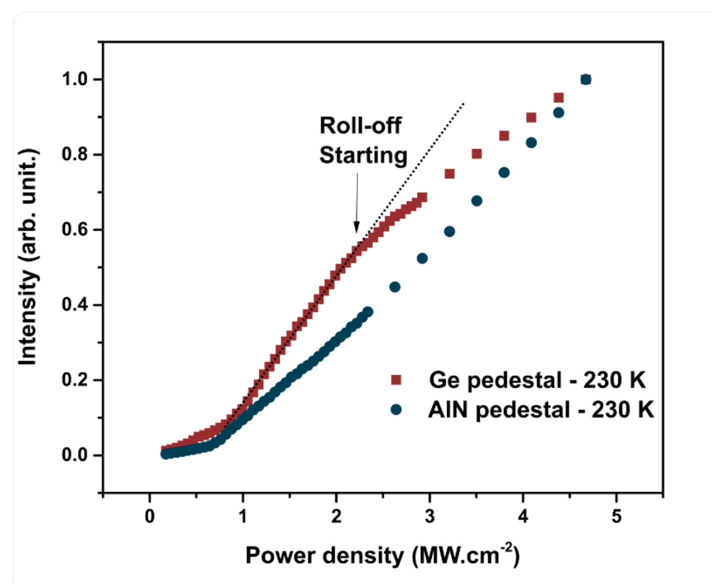

FIG. S3. Normalized L-L curves at 230K for GeSn disk on Ge (red square) and on AlN (blue circle).

At 230 K, a roll-off is clearly visible on the L-L curve (**Fig. S3**) for GeSn disk on Ge, which comes with a heating of the suspended structure. On the other hand, the L-L curve for the GeSn disk with AlN pedestal at the same cryostat temperature does not present a roll-off, in line with improved heat transport in this case. Roll-off and thus heating start to appear for the disk with the AlN configuration at 245 K. This is clearly visible at 260 K (**Fig. S4**), which is in good agreement with the mean 24 K thermal shift deduced from fig 4a.

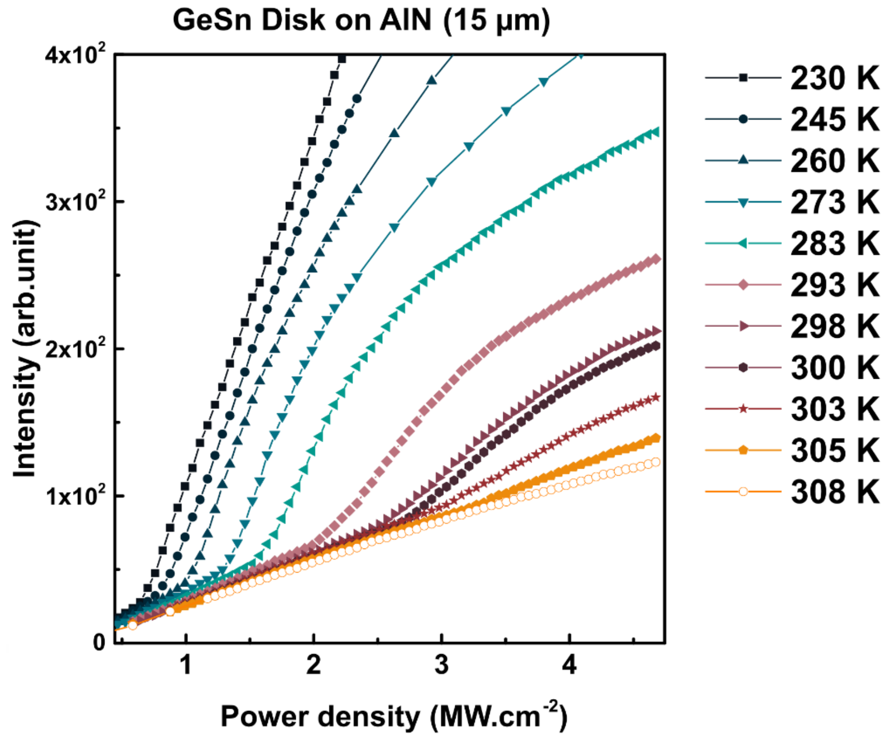

FIG. S4. L-L curves for the GeSn disk on AlN. Same figure is presented in the main article but here linear scales were set to clearly observe the apparition of a roll-off between 245 K and 260K.

D. Details on the simulation of GeSn 17.2% optical gain

The band structure of relaxed GeSn 17.2%, with energy levels and wave-functions fed into optical gain simulations, was calculated using the empirical pseudopotential method (**Fig. S5**). The pseudopotential was fitted to reproduce the reference values of direct gap, indirect gap and the spin-orbit gap of relaxed GeSn 17.2%[6]. An offset of -70 meV was added into the conduction band energies to simulate the effect of band gap narrowing at room temperature, based on the photoluminescence data of high Sn concentration GeSn at different temperatures (not shown here). The values taken in this work for GeSn 17.2% direct gap, indirect gap and spin-orbit gap at room temperature are 0.245 eV, 0.421 eV and 0.379 eV, respectively.

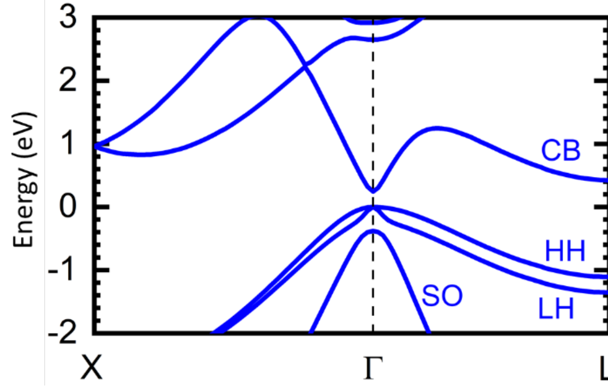

FIG. S5. Band structure of GeSn 17.2% at room temperature, calculated using the empirical pseudopotential method. CB, HH, LH, SO stand for conduction band, heavy-hole band, light-hole band and spin-orbit band, respectively.

For the calculation of optical gain, the following formula was used to extract the band-to-band gain/absorption:

$$\alpha(\hbar\omega) = \frac{\pi e^2}{n_r c \varepsilon_0 m_0^2 \omega} \int_{k\epsilon BZ} \frac{d^3k}{(2\pi)^3} \sum_a \sum_b |\hat{\boldsymbol{e}}.\boldsymbol{p}_{ba}|^2 \delta(E_b(k) - E_a(k) - h\omega)(f_a - f_b) \quad (S1)$$

with the definition for each term detailed in Ref. 6. The Dirac distribution was replaced by a Gaussian function with a full width at half maximum (FWHM) of 25 meV. The integral was discretized on the first Brillouin zone (BZ), using a grid with a 240 x 240 x 240 resolution to ensure simulation convergence. The free carrier absorption was modelled using Liu *et al.* empirical formula for Ge[7], extended here for GeSn:

$$\alpha_{FCA}(\lambda) = -3.4\ 10^{-25} n\ \lambda^{2.25} - 3.2\ 10^{-25} p\ \lambda^{2.43} \quad (S2)$$

n, p being the injected electron/hole density in cm^{-3}, λ the photon wavelength in nm and α_{FCA} the free carrier absorption in cm^{-1}.

We show, in **Fig. S6,** a complete set of data for the evolution of net gain spectra as a function of the temperature, with data at 303 K, 313 K and 333 K in addition to the data at 293 K, 323 K and 343 K already shown in **Fig. 4(b)** of the manuscript.

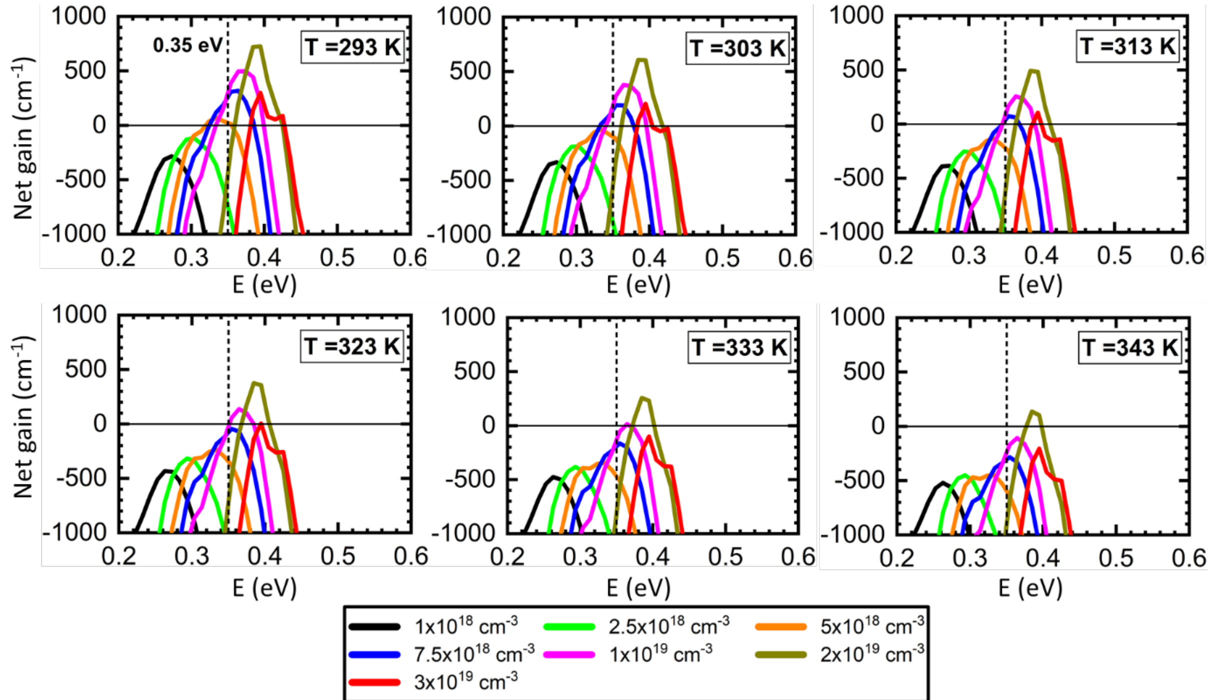

FIG. S6. Computed net gain of relaxed GeSn 17.2% as function of the photon energy, at different values of n_{inj} between 1×10^{18} cm^{-3} and 3×10^{19} cm^{-3}, between 293 K and 343 K.

REFERENCES

[1] Q.M. Thai, N. Pauc, J. Aubin, M. Bertrand, J. Chrétien, V. Delaye, A. Chelnokov, J.-M. Hartmann, V. Reboud, and V. Calvo, Opt. Express, **26**, 32500 (2018).
[2] J. Chrétien, N. Pauc, F. Armand Pilon, M. Bertrand, Q.-M. Thai, L. Casiez, N. Bernier, H. Dansas, P. Gergaud, E. Delamadeleine, R. Khazaka, H. Sigg, J. Faist, A. Chelnokov, V. Reboud, J.-M. Hartmann, and V. Calvo, ACS Photonics, **6** (10), 2462–2469 (2019).
[3] J. Aubin, J.M. Hartmann, A. Gassenq, J.L. Rouviere, E. Robin, V. Delaye, D. Cooper, N. Mollard, V. Reboud, and V. Calvo, Semicond. Sci. Technol. **32**, 094006 (2017).
[4]D. Spirito, N. von den Driesch, C.L. Manganelli, M.H. Zoellner, A.A. Corley-Wiciak, Z. Ikonic, T. Stoica, D. Grützmacher, D. Buca, and G. Capellini, ACS Applied Energy Materials, **4**, 7, 7385–7392 (2021)
[5] Y. Kim, S. Assali, D. Burt, Y. Jung, H.-J. Joo, M. Chen, Z. Ikonic, O. Moutanabbir, and D. Nam, Avanced Optical Material, 2101213 (2021).
[6]M. Bertrand, Q.-M. Thai, J. Chrétien, N. Pauc, J. Aubin, L. Milord, A. Gassenq, J.-M. Hartmann, A. Chelnokov, V. Calvo, and V. Reboud, Annalen Der Physik **531**, 1800396 (2019).
[7]J. Liu, X. Sun, D. Pan, X. Wang, L.C. Kimerling, T.L. Koch, and J. Michel, Opt. Express, **15**, 11272 (2007).